FRONTIERS OF PHYSICS

TOPICAL REVIEW
Volume 18 / Issue 4 / 43603 / 2023

Insight into the growth mechanism of black phosphorus

Yongjie Wang[1,2], Qiang Yu[2], Jie Li[2], Junyong Wang[2], Kai Zhang[2,†]

1 Nano Science and Technology Institute, University of Science and Technology of China, Suzhou 215123, China
2 CAS Key Laboratory of Nanophotonic Materials and Devices & Key Laboratory of Nanodevices and Applications, i-Lab, Suzhou Institute of Nano-Tech and Nano-Bionics (SINANO), Chinese Academy of Sciences, Suzhou 215123, China
Corresponding author. E-mail: †kzhang2015@sinano.ac.cn
Received November 9, 2022; accepted February 7, 2023

ABSTRACT

Two-dimensional (2D) black phosphorus (BP) has attracted great attention in recent years in fundamental research as well as optoelectronics applications. The controllable synthesis of high-quality BP is vital to the investigation of its intrinsic physical properties and versatile applications. Originally, BP was mostly synthesized under high temperatures and pressures. Subsequently, metal flux, wet chemical and chemical vapor transport (CVT) methods had been appeared successively. The pulsed laser deposition (PLD) and CVT methods have been used to prepare high-quality BP thin films on silicon substrates, which is significant for its monolithic integration and practical applications. To meet the demand of the scalable applications of BP, the direct preparation of BP films on dielectric substrates that avoids additional transfer process, is crucial to high-performance device implementation. In this review, the growing methods and corresponding mechanisms of BP are summarized and analyzed. Meanwhile, the view on the controllable growth of large-area, high-quality BP films is envisioned.

Keywords black phosphorus, growth mechanism, nucleation, thin films

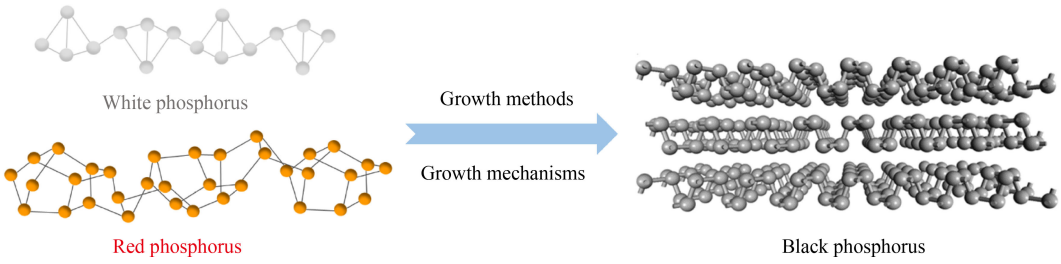

Contents

*Special Topic: Black Phosphorus and Its Analogues (Eds. Xianhui Chen, Haibo Zeng, Han Zhang & Yuanbo Zhang).

Higher Education Press

https://doi.org/10.1007/s11467-023-1265-7

1 Introduction

In recent years, two-dimensional (2D) phosphorus have attracted much attention as an elemental 2D material due to its intriguing properties. There are several allotropes of elemental phosphorus [1–4], namely white phosphorus, red phosphorus (RP), violet phosphorus, and black phosphorus (BP). White phosphorus is a light yellow wax-like and translucent crystalline solid that glows in the dark and is easy to spontaneously ignite [5, 6]. RP is a dark red powder, insoluble in water, and its chemical properties are relatively stable [7–10]. Violet phosphorus was first found by Hittorf in 1865 with the observed color of purple, so it was named as Hittorf's phosphorus (HP) as well [11]. The basic building block of violet phosphorus is a tubular structure composed of $-P_2-P_8-P_2-P_9-$ cycles, which are arranged in parallel in a plane [12–15]. BP is a black crystal with a metallic luster. It has the weakest reactivity among the allotropes of phosphorus [16–19]. Compared with other allotropes of phosphorus, BP is a layered crystal and has excellent electrical and optical properties which has attracted increasing interest since the rising of 2D layered materials.

BP was first synthesized and discovered in 1914 [20]. The crystal structure of BP is orthorhombic under ambient temperature and pressure, the space group is Cmca, $a = 3.313$, $b = 10.473$, $c = 4.374$. Figure 1(a) shows the atomic structure of three-layer BP in top and side view [21, 22], phosphorus atoms are connected and arranged in a wrinkled shape. BP is a layered structure, phosphorus atoms in the same layer are not in the same plane, showing a honeycomb fold structure. There are strong covalent bonds within the layers and atoms between layers are connected by van der Waals interactions. The distance between two layers is about 5 Å. Because of

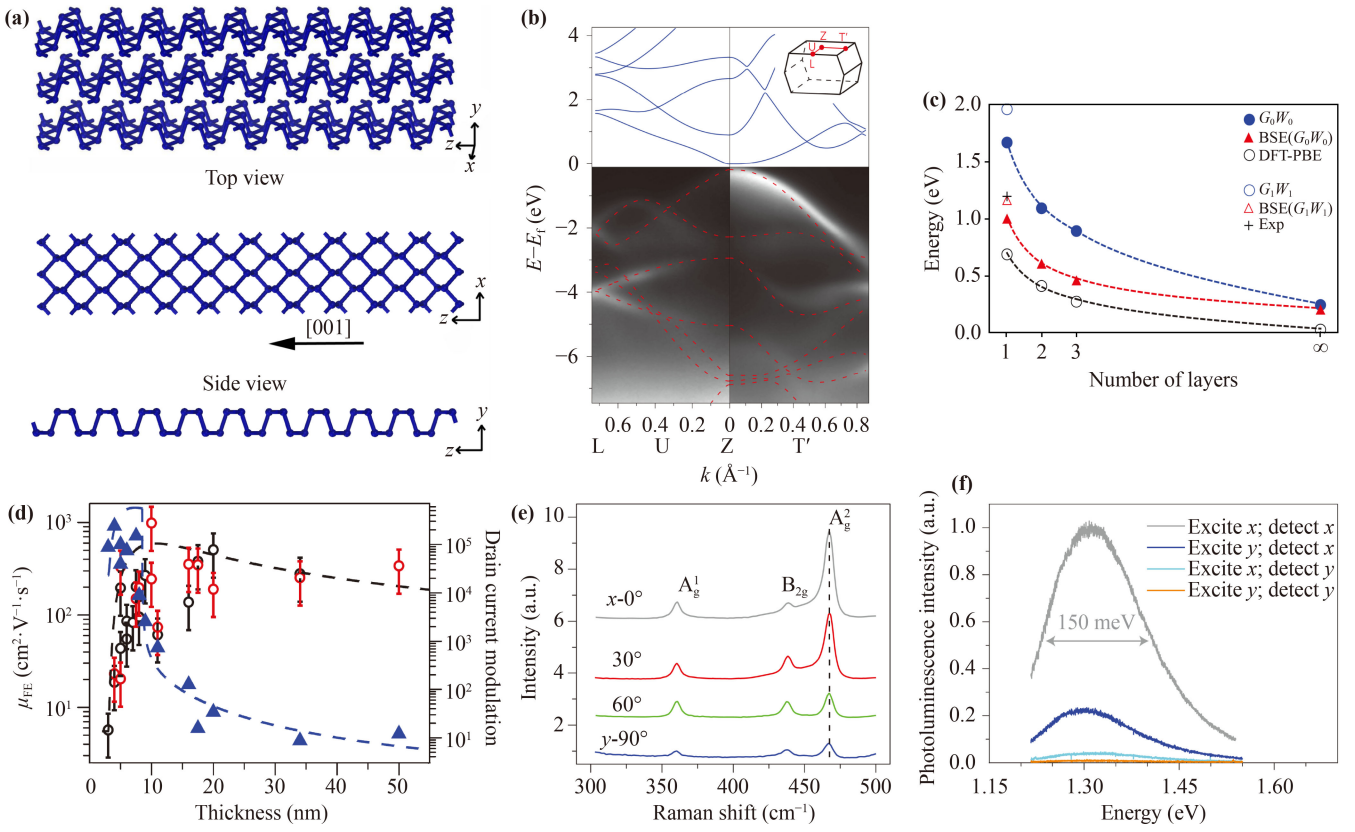

Fig. 1 **(a)** Schematic diagram of the structure of three layers of BP, top view of layered BP and side view of layered BP. **(b)** The band structure of bulk BP measured by ARPES, above which is the band calculation of the bulk crystal. **(c)** Band gaps of BP with different layers are calculated by different functional models. **(d)** The field-effect mobility is measured for devices with different thicknesses. **(e)** Polarization resolved Raman scattering spectra of monolayer BP with linearly polarized laser excitation. **(f)** Polarization-resolved photoluminescence spectra of monolayer BP, revealing the excitonic nature of emission from the monolayer BP. Reproduced with permission from Ref. [22] (a), Ref. [23] (b), Ref. [24] (c), Ref. [23] (d) and Ref. [60] (e, f).

this layered BP structure, single or few layers BP films could be obtained from a bulk crystal by mechanical or liquid exfoliation.

Bulk BP is a semiconductor with a direct bandgap of ~0.3 eV, as shown in the angle-resolved photoemission spectroscopy (ARPES) measurement in Fig. 1(b) [23]. Interestingly, the band gap of BP thin film is related to its layer number [24], as shown in Fig. 1(c). As the number of BP layer decreases, the band gap of BP gradually increases. The band gap of monolayer BP can reach to 2.0 eV. Besides, BP is a high-carrier mobility semiconductor at room temperature, and the charge-carrier mobility is found to be thickness-dependent [25–29]. When the thickness is about 10 nm, the carrier mobility value can reach 1000 $cm^2 \cdot V^{-1} \cdot s^{-1}$, as shown in Fig. 1(d). Therefore, BP film has great potential in the application of 2D nano-electronic devices. Due to the reduced in plane symmetry of its structure, BP exhibits anisotropic physical properties. Through the test of polarized Raman spectroscopy and polarized photoluminescence of BP, as shown in Figs. 1(e) and (f), the anisotropy of lattice vibration and exciton are observed.

Based on the above characteristics, the application of BP in many fields has been widely reported, such as transistors [23, 30, 31], photonics [32], optoelectronics [33–35], sensors [36, 37], batteries [38–40], and catalysis [41]. Especially in the field of photodetection, the direct, narrow and thickness-dependent bandgap of BP provides a platform for developing high-performance mid-infrared photodetectors, which is distinctly superior to other 2D materials. Many good reviews have summarized this [42–44]. Moreover, due to the efficient interaction and good compatibility with biological cells, BP plays an important role in biomedicine [45–47], they gradually degrade into non-toxic small molecular weight substances in biological cells and reacts to produce phosphate, in which phosphorus is involved in almost all cellular processes. However, the instability of BP under ambient condition [48–51]and uncontrollable preparation of large-scale BP films [52, 53] greatly hinder its development and practical application.

The acquisition of large-area and high-quality few-layer BP is essential for the fabrication of functional devices. Since the first discovery of graphene, the mechanical exfoliation method has unleashed a new research field. It promotes the study of various 2D materials [54]. Similarly, different layers of BP can be obtained by exfoliating the bulk crystal. The preparation of few-layer BP was reported in 2014 [55], which was achieved by micromechanical cleavage followed by transferring onto SiO_2/Si substrates. So far, this method remains the main method to obtain BP thin films for applications in microelectronic devices. Besides mechanical exfoliation, another strategy was proposed by etching larger-area thick BP flakes to the 2D limit by Ar^+ plasma [56]. Subsequently, several other exfoliation methods of BP have also been developed for optoelectronic devices [57–59], but the area and layers obtained are not controllable and the yield is limited. In order to accelerate the docking of large-scale applications, a bottom-up method to control the growth of large area and few layers of BP on silicon substrate is the direction of future development. Therefore, it is of great significance to summarize and explore the growth mechanism of preparing BP and its thin film.

Over the past few decades, various growth methods of BP have been rapidly developed and updated. In this review, we begin with the fundamental structures and the properties of BP. Then we give a comprehensive review about the recent progress in the controllable growth of bulk BP. Lastly, corresponding growth mechanisms of BP were described.

2 Preparation method of bulk BP

2.1 Phase transformation under high temperature and high pressure

The high temperature and high pressure (HTHP) method is the earliest method for preparing BP. It was developed by Bridgman in 1914 [20]. Schematic diagram of the experimental setup is shown in Fig. 2(a). White phosphorus and RP powder are placed in a cylindrical boron nitride sample tube. Then, the cylindrical BP is obtained at a pressure of 2.0–5.0 GPa and temperature of 200–800 °C. BP powder can be further obtained by grinding, as shown in Fig. 2(b) [61]. The HTHP method can also be utilized to realize the doping of BP, such as doping germanium, sulfur and selenium [62], which can further improve its optoelectronic properties and stability.

Detailed and systematic study on the preparation of BP by HTHP method have been investigated [63, 64]. BP prepared at different temperatures and pressures was characterized by XRD patterns and Raman spectra. The results show the differences in the crystallite size and crystallinity of BP. The phase transition even occurs when the pressure exceeds 4.5 GPa. Pressure is more significant to the transformation than temperature.

There are layered semiconducting orthorhombic (A17) phase, layered semimetallic rhombohedral phase (A7) [65] and non-layered simple cubic phase in BP [66]. BP is A17 at room temperature and atmospheric pressure. When the pressure varies from ordinary pressure pressurized to 30.0 GPa, the phase structure of BP can be transformed to A7 and simple cubic phase, as shown in Fig. 2(c). With the pressure increasing, the XRD pattern shows that the peak positions of A17, A7 and simple-cubic phase have been deviated, indicating that the phase transition occurs, as shown in Fig. 2(d).

Although the HTHP method can be used to prepare BP single crystals, the experimental conditions are dangerous and involves sophisticated and expensive equipment. As a result, it is not conducive to large-scale production.

2.2 Mercury catalysis and metal flux

In 1955, Krebs *et al.* [67] used metallic mercury and white phosphorus as precursors to prepare BP single crystals. In this method, metallic mercury can reduce the required temperature, pressure and activation energy threshold for the conversion of white phosphorus to BP. The metal mercury and white phosphorus are mixed into an autoclave, and the reaction temperature is 380–480 ℃ with a holding time about 3 days. This method has been rarely further studied due to the highly toxic metallic mercury. In 1965, Brown [68] used the liquid bismuth auxiliary method which convert white phosphorus into BP at a certain temperature. They purified white phosphorus in 15% HNO_3, dissolved it in liquid bismuth, then heated it to 400℃ and cooled it slowly to room temperature. Because RP is insoluble in liquid bismuth, RP is converted into white phosphorus by the device shown in Fig. 3(a). In these processes bismuth is first preheated to 300 ℃ [Fig. 3(a)], and then, the bismuth and white phosphorus were heated to 400℃ for 20 h. Finally, needle-shaped or rod-shaped BP crystals are obtained. It is a new method for preparing BP which avoids the strict requirements of the HTHP method on the reaction equipment. However, this method has been rarely used at present as well due to the toxicity of bismuth and low yield of BP.

2.3 Ball milling

The high-energy ball milling method, also known as the mechanochemical method, relies on the rotation of the ball to impact the powder to nanoparticles. The huge mechanical energy was produced in a short time which is beneficial to the phase transition [69]. Under the action of mechanical force, RP generate phase transition then convert into BP. The pressure on the sample

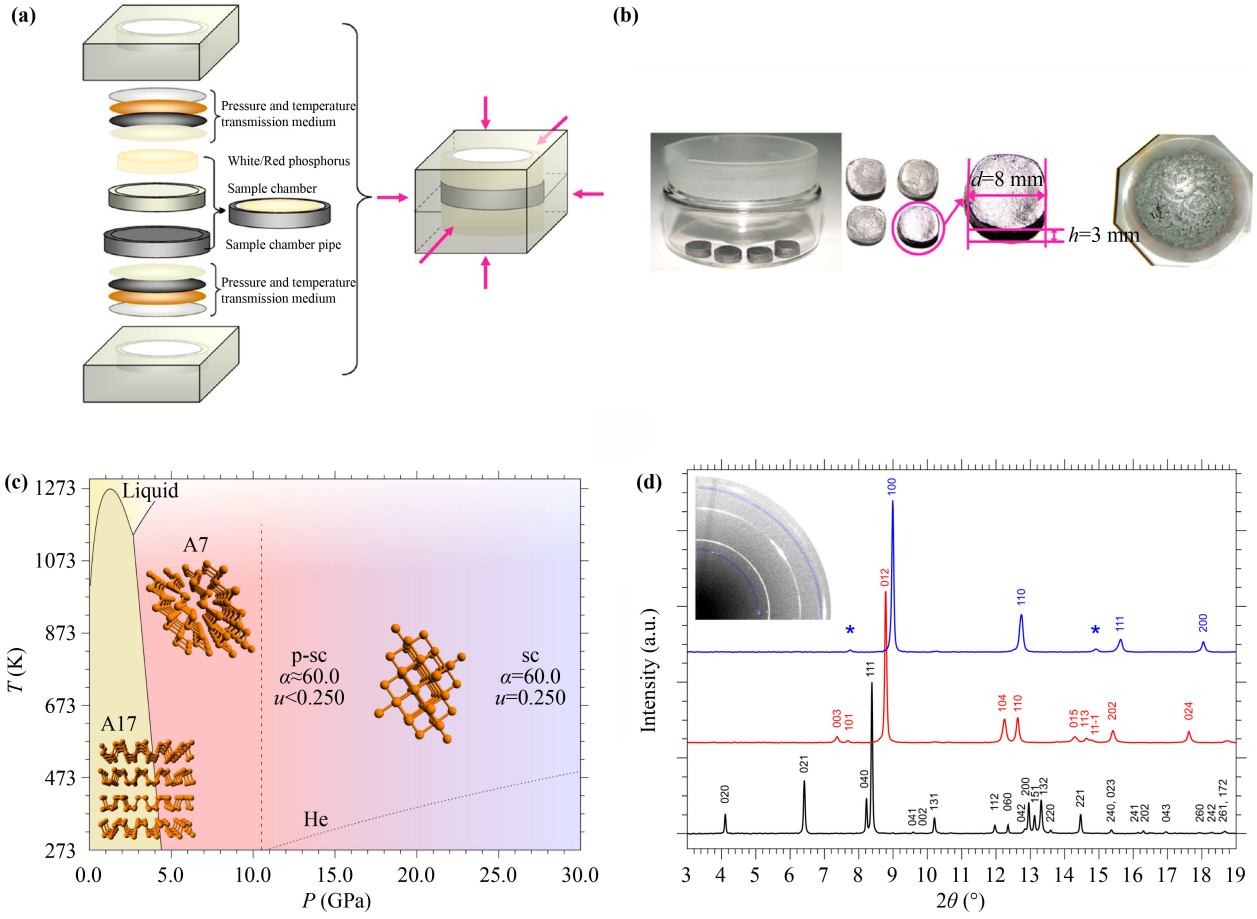

Fig. 2 **(a)** The schematic diagram of the experimental setup used to produce BP. **(b)** Photograph of the BP sample. **(c)** Phase diagram of phosphorus between 0 GPa to 30.0 GPa, showing the pressure and temperature ranges where A7, A17 and simple-cubic are reported to be stable. **(d)** The XRD patterns of phosphorus at room temperature are the A17 phase at 0.2 GPa (black trace), the A7 phase at 6.5 GPa (red trace), and the simple-cubic phase at 11.2 GPa (blue trace), showing the shifts in peak positions. Reproduced with permission from Ref. [61] (a, b) and Ref. [66] (c, d).

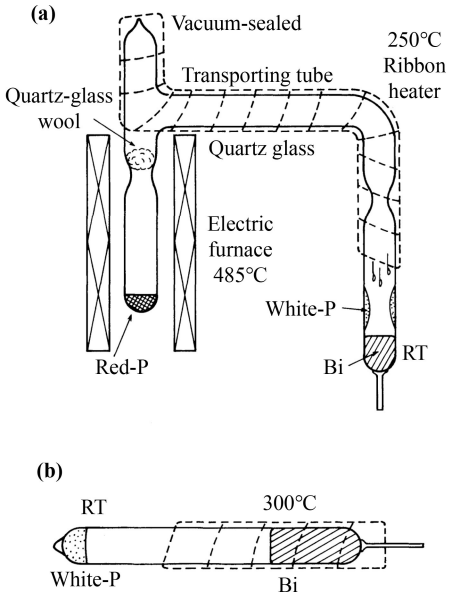

Fig. 3 **(a)** Quartz-glass apparatus for the transformation of Red-P to White-P. **(b)** Quartz-glass ampoule for crystallization of BP. Reproduced with permission from Ref. [68].

powders formed between the balls and the vessel wall is the main factor affecting the transformation process of RP to BP. Hence, the different ratios of steel balls and powder and different ball milling times were tested. Three groups of samples were selected to conduct experiments at different ball milling times [70]. The larger ratio of steel balls and powder, the larger the instantaneous energy that can be obtained. Moreover, the longer ball milling time, the easier it is to prepare BP, as shown in Fig. 4(a).

The thickness of BP nanosheets prepared by ball milling is widely distributed. As shown in the XRD spectra of the product obtained at different grinding time [Fig. 4(b)]. The crystallinity of the sample depends on the time of ball milling and the ratio of balls and PR powder. If adding some additives, such as LiOH, the doped-BP by ball milling can react as a photocatalyst with a higher yield of hydrogen evolution [71], as shown in Fig. 4(c). Therefore, the element doped and substituted of BP can be realized by ball milling. Another example is adding Sn and RP in a ball mill, where Sn-doped BP was obtained and its electrical conductivity was improved [72]. Figures 4(d) and (e) are the SEM images of BP prepared by ordinary ball milling and adding additives, respectively. The bulk BP has a lamellar structure with uneven size, and most of the lamellae are larger than 10 μm in lateral dimension. The particle size of BP was greatly reduced (300–500 nm) after ball milling with additives.

2.4 Wet chemical method

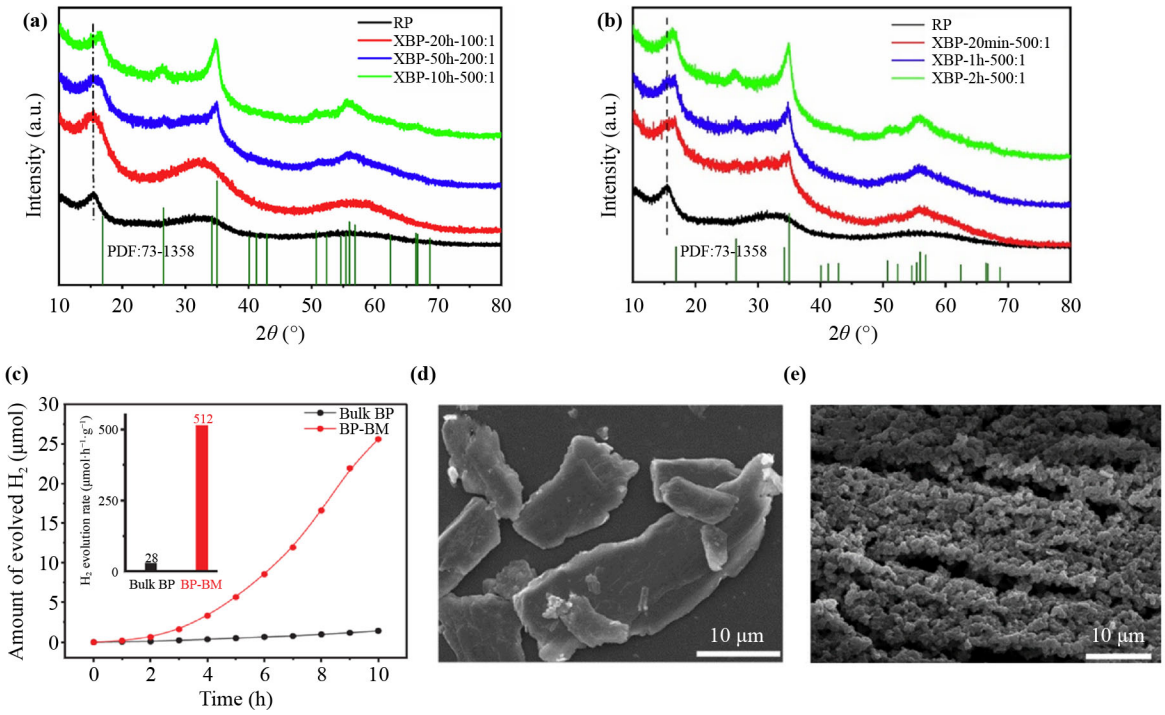

Fig. 4 **(a)** The XRD pattern of the samples synthesized by planetary milling under different conditions. **(b)** The XRD pattern of samples by shake milling for different milling time. **(c)** H_2 production rate of BP obtained by ordinary ball milling and BP obtained by adding catalyst. **(d)** and **(e)** are the SEM images of bulk BP and BP obtained by ball milling with additives. Reproduced with permission from Ref. [70] (a, b) and Ref. [71] (c–e).

BP nanosheets have been synthesized by wet chemical method [73]. White phosphorus (raw material) and ethylenediamine (solvent) are mixed into a reaction kettle, product will be obtained under 60–140 ℃. The X-ray diffraction (XRD) of the prepared powder samples confirms that the orthorhombic crystal structure of BP without other phases, and the typical Raman peaks are located at 360.2 cm^{-1}, 437.5 cm^{-1}, and 464.6 cm^{-1}. Lattice images of BP nanosheets show an orthogonal BP (020) plane spacing of 0.507 nm.

Solvent and temperature are two key factors in the wet chemical method synthesis of BP nanosheets. They can control the formation of BP nanosheets and their thickness. White phosphorus initially forms layered RP with the aid of ethylenediamine at room temperature. Then RP is more active in hot solution and ethylenediamine molecules enter the RP layer. Under the action of heating, the multi-layer RP nanosheets are exfoliated into few-layer RP nanosheets. Meanwhile, during the exfoliation process, the RP was further transformed into the BP phase.

Furthermore, wet-chemical approach can obtain BP nanosheets loaded with amorphous cobalt phosphide (Co–P) nanoparticles. In the hydrothermal synthesis process, Co^{2+} will react with P atom to form Co–P nanoparticles on the surface of BP nanosheets, which act as photocatalysts [74], as shown in Fig. 5(a). By comparing the XRD of pure BP, the product prepared via solvothermal method showed a typical BP orthorhombic structure, and no other phases were detected, as shown in Fig. 5(b). The XRD peaks are weaker and broader, showing lower crystallinity and smaller size, which is beneficial to improve the photocatalytic activity. Because more defects are easily formed in the samples prepared via the wet chemical route. The Raman spectra of the two samples shows similar spectral distributions, with Raman peaks between 300 and 500 cm^{-1}. In general, three of them are characteristic Raman peaks of BP: A_g^1 (365 cm^{-1}), B_g^2 (442 cm^{-1}), A_g^2 (470 cm^{-1}), as shown in Fig. 5(c). It further suggests that BP nanosheets and Co–P nanoparticles can be prepared via the wet-chemical approach.

2.5 Chemical vapor transport

The chemical vapor transport (CVT) reaction is an important and traditional synthetic method for the growth of pure crystalline solids. The CVT reaction involves three processes: sublimation, transport and deposition. Firstly, the solid sublimes in the presence of

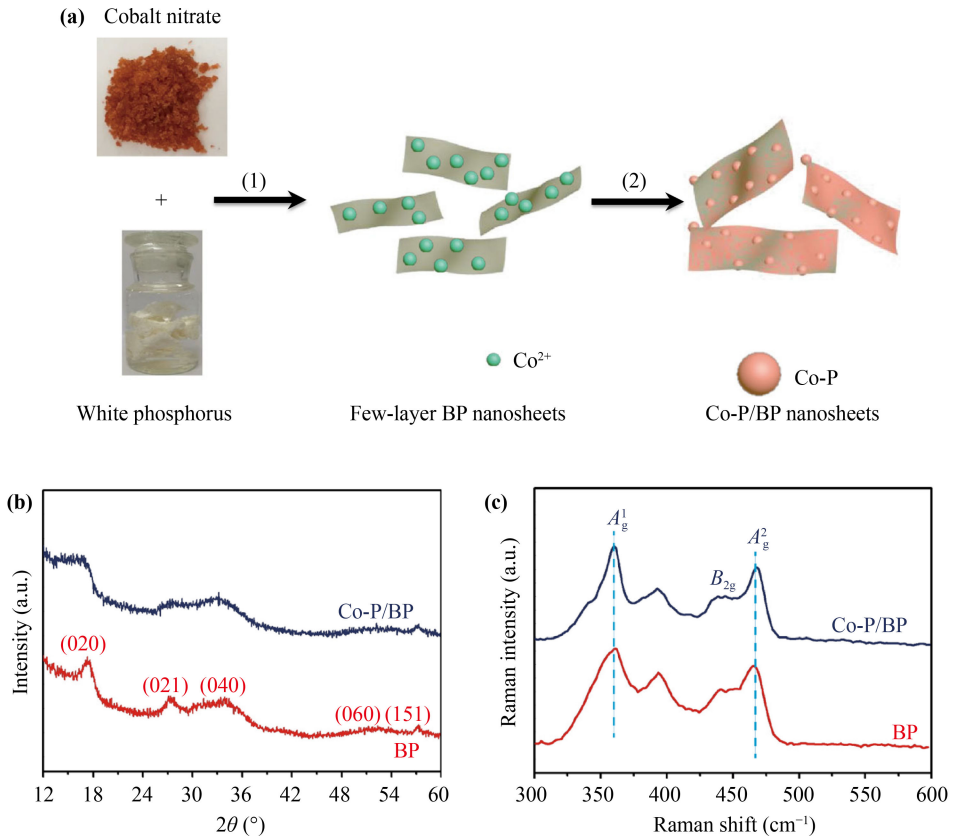

Fig. 5 **(a)** Multilayer BP nanosheets prepared by solvothermal reaction of white phosphorus and Co^{2+} in ethylene diamine, the formation mechanism of amorphous Co–P nanoparticles. **(b)** XRD patterns of the BP (red line) and Co–P/BP (navy line) samples. **(c)** Raman spectra of the pristine BP and Co–P/BP samples. Reproduced with permission from Ref. [74].

a gaseous reactant (the mineralizer). Then gaseous precursors are transported under the action of temperature gradients. Finally, gaseous precursors usually deposit elsewhere in the form of crystals. This method is typically used to obtain crystal with low defect density and high crystal quality.

By using RP, gold (Au), tin (Sn) and tin iodide (SnI_4) as raw materials, BP can be prepared via heating and cooling for a period of time under low pressure conditions. The Au_3SnP_7, AuP and Sn_4P_3 appeared together with BP. This new preparation method is simple and effective which can avoid complicated preparation devices and toxic catalysts and is of great significance in the process of preparing BP. According to the structural features of BP and Au_3SnP_7, the possible formation mechanism is discussed. BP was grown on the Au_3SnP_7, as shown in Fig. 6(a). At the same time, the ternary phase diagram composed of Au, Sn and P was studied, as shown in Fig. 6(b). A comparison of the crystal structures of the BP and Au_3SnP_7 reveals some interesting topological features in these two materials, as shown in Fig. 6(c). Under certain pressure and temperature, Au_3SnP_7, BP and RP exist successively in their own phase region, as shown in Fig. 6(d). The RP evaporates into P_4 at higher temperatures, then P_4, Sn and Au form Au_3SnP_7 at the first time. At lower temperatures, P_4 will be converted to BP. This demonstrates that growth of BP on Au_3SnP_7 is at least possible. It played an important role in the conversion from RP to BP crystals. They can reduce the growth time by using the AuSn alloy instead of Au and Sn metals. This is called AuSn/SnI_4/RP reaction system [75]. Because Au is relatively expensive, and it was later found that BP can be successfully prepared by using only Sn, I_2 and RP. Therefore, there are few articles on the preparation of BP by Au, Sn, I_2 and P.

Recently, BP has been reported to be synthesized by mineralizer-assisted vapor transport reactions at lower pressures. The initial reported mineralization additive was Au, Sn and SnI_4, which was then simplified to Sn and SnI_4, that is RP/Sn/I_2 system [77–80]. It not only reduced the synthetic cost of BP single crystals but also further reduced the unwanted phases. When BP was prepared with RP, I_2 and Sn as raw materials, the $Sn_{24}P_{19.3}I_8$ was found as BP nucleating agent [81]. A brown substance was found at the bottom of BP and characterized by XRD, it was proven to be $Sn_{24}P_{19.3}I_8$. In order to further investigate whether $Sn_{24}P_{19.3}I_8$ would help RP transform into BP, HRTEM was used to clarify whether there is a distinct phase boundary between BP and $Sn_{24}P_{19.3}I_8$. It is found that the (040) plane of BP

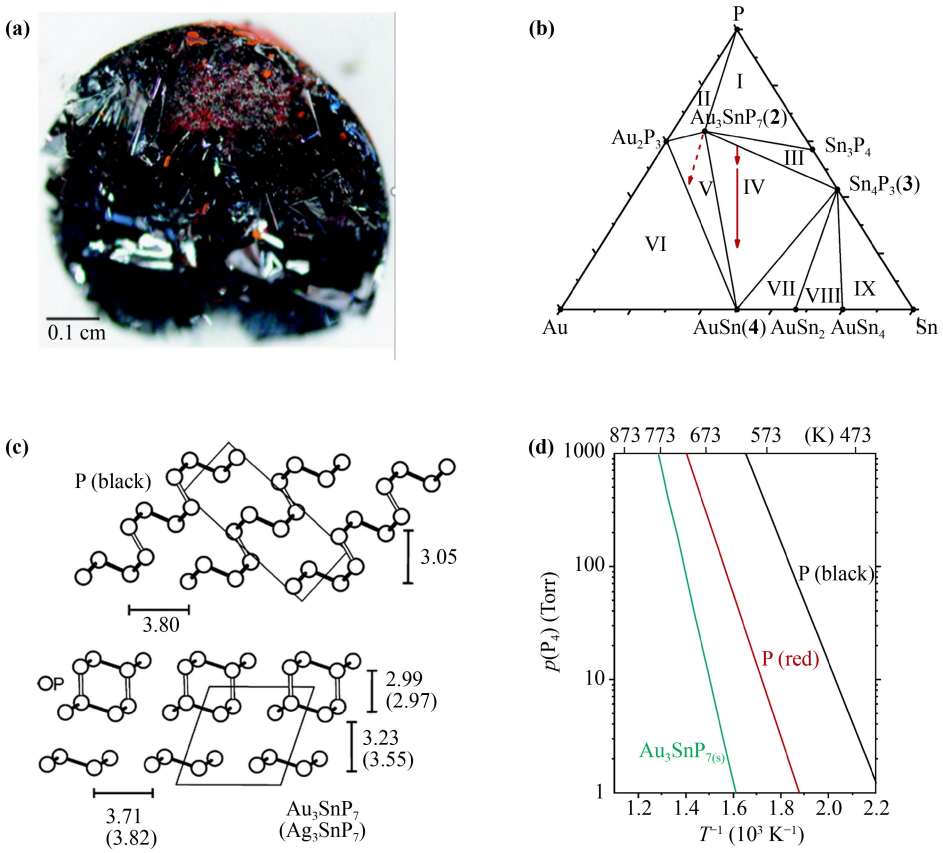

Fig. 6 **(a)** The presence of Au_3SnP_7/AuSn near the growth of BP. **(b)** Ternary phase diagram of Au, Sn and P. **(c)** Sections of the P substructures of BP (view on (100), top part), and Au_3SnP_7 (view on (010), bottom part). **(d)** Phase barogram of the Au/Sn/P system (873 K). Reproduced with permission from Ref. [76].

and the (200) of $Sn_{24}P_{19.3}I_8$ form a clear phase boundary. It is a powerful evidence to confirm that $Sn_{24}P_{19.3}I_8$ is the nucleation agent. The unit structures of $Sn_{24}P_{19.3}I_8$ and BP both contain P atoms, and they both share some similar topological features. It also explains the possibility that $Sn_{24}P_{19.3}I_8$ is the nucleation point.

The $Sn_{24}P_{19.3}I_8$ belongs to $Pm\bar{3}n$ space group [82] whose basic building unit is a 3D network which composed of tin atoms and phosphorus atoms. Each P atom is further combined with three tin atoms which forms complete twisted tetrahedral coordination. It was reported that tin atoms and phosphorus atoms occupy two crystal positions which form a framework [83], and iodine atoms occupy the center of the polyhedral cage respectively. The polyhedron of the crystal structure is presented in Fig. 7(a). The coordination structure formed by P atoms and Sn atoms is shown in Fig. 7(b).

It has been suggested that the intrinsic P vacancies in the ternary clathrate $Sn_{24}P_{22-x}I_8$ framework are important for the growth of BP [84]. The P vacancies in the $Sn_{24}P_{22-x}I_8$ solid can greatly enhance atomic diffusion, as shown in Fig. 8(a). According to the speculation, the growth mechanism of BP crystals may be explained by vapor-solid-solid model. Figure 8(b) shows that $Sn_{24}P_{22-x}I_8$ is a three-dimensional inverse structure. It composed of Sn and P atoms as host skeletons and Iodine as guest atoms. Through characterized by XRD and compared with the standard PDF card, it is proved that the substance is $Sn_{24}P_{22-x}I_8$, as shown in Fig. 8(c). BP can be prepared by using $Sn_{24}P_{22-x}I_8$ and RP, and

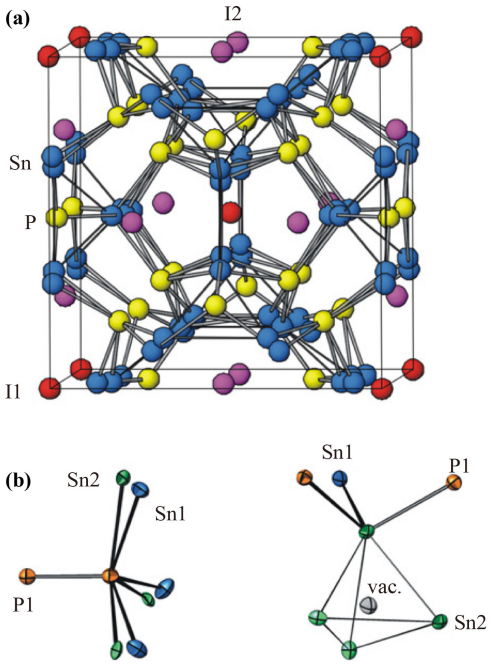

Fig. 7 A presentation of the crystal structure of $Sn_{24}P_{19.3}I_8$. **(a)** A view of the unit cell of $Sn_{24}P_{19.3}I_8$. **(b)** Unit structure composed of P and Sn. Reproduced with permission from Ref. [83].

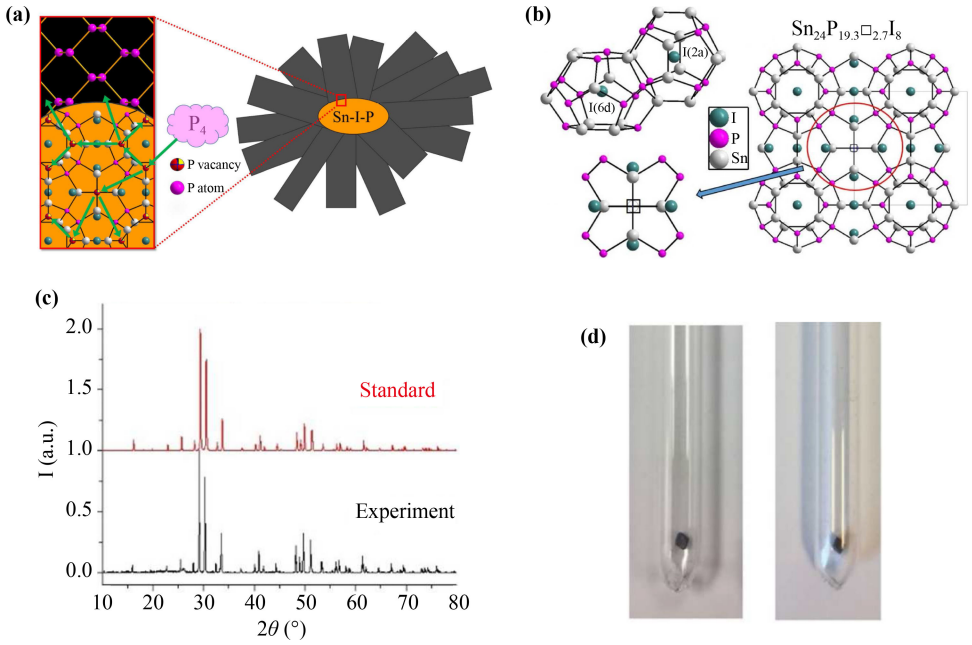

Fig. 8 **(a)** The orange part represents the ternary compound of $Sn_{24}P_{22-x}I_8$; the black part represents BP; the purple dots represent P atoms; the colorful dots represent P vacancies; the green dots represent I atoms; and gray dots represent Sn atoms. The green arrows indicate the possible diffusion path of P atoms with the assistance of P vacancies. **(b)** Pentagonal dodecahedra and tetrakaidecahedron framework formed by Sn and P atoms in the clathrate $Sn_{24}P_{22-x}I_8$. **(c)** The XRD pattern of $Sn_{24}P_{22-x}I_8$. **(d)** Pictures of a $Sn_{24}P_{22-x}I_8$ pellet inside the reaction ampule before and after 550 °C, showing $Sn_{24}P_{22-x}I_8$ remains unchanged. Reproduced with permission from Ref. [84].

the temperature of the whole reaction process is 550 °C. In addition, another experiment demonstrated that $Sn_{24}P_{22-x}I_8$ particles remained unchanged from room temperature to 550 °C, as shown in Fig. 8(d). The successful preparation of BP with $Sn_{24}P_{22-x}I_8$ and RP was under 520 °C. It shows that $Sn_{24}P_{22-x}I_8$ did not decompose during the growth of BP, which further proves the vapor-solid-solid mode.

BP bands can grow radially from a core, making the grown BP look like a sea urchin. It suggests that BP grows along a nucleation site and grows around [85]. In addition, $Sn_{24}P_{19.3}I_8$ acts as a nucleating agent, BP grows slowly on this nucleating agent and form large crystals. During the reaction process of growing BP, a phase transition occurs between RP, HP and BP. The synthesis of BP is a step-by-step phase transformation process, and at different temperature stages, substances through different phase transformation.

The element of RP, Sn and I form gray solid solutions that including $Sn_{24}P_{19.3}I_8$ and Sn_4P_3, HP converts to BP under the action of gray melt [86]. The element P in the $Sn_{24}P_{19.3}I_8$ and Sn_4P_3 compounds can be separated out and then form HP in the cold zone. Then $Sn_{24}P_{19.3}I_8$ and Sn_4P_3 decompose, Sn and I will come out, and then they will react with the remaining gas P again to continue to form $Sn_{24}P_{19.3}I_8$ and Sn_4P_3. When element P is completely transformed into HP, $Sn_{24}P_{19.3}I_8$ and Sn_4P_3 are adsorbed on its surface, which can act as catalytic sites to convert HP into crystalline BP. The phase interface between HP and BP also shows the possibility of the transition from HP to BP.

In order to reveal the effect of different mineralizers, Sn was substituted by lead (Pb) in the reaction system [87]. By using Pb, I_2 and RP as raw materials, the CVT method was used to synthesize BP [88]. The BP prepared by using Pb, I_2 and RP is characterized by XRD and Raman spectrum, it confirmed the successful preparation of BP crystals. There is no impurity on BP, and it also has better electrical properties. It was proved that higher purity BP could be obtained by replacing tin with Pb. Through STEM-EDX spectra confirmed Sn in Sn-BP, but no Pb impurity was found in Pb-BP. Due to the toxicity of Pb, there is unsafe during the experiment. However, this experiment also proved that this method can prepare BP, and provided another method for preparing BP with a mineralizer which avoided impurities and had good electrical properties.

3 Exploration on the preparation of BP films

Although great breakthrough has been made in the preparation of bulk BP, few-layer BP films growth is still a great challenge, most few-layer BP films can only be obtained by mechanical exfoliation of bulk BP so far. While, the BP films obtained by mechanical exfoliation encounters the problems of limit size, uncontrollable layer number and low yield. It is expected that BP films can be grown directly on the desired substrates.

3.1 Epitaxial nucleation

Xu *et al.* [89] achieved the growth of BP films on buffer by firstly forming Au_3SnP_7 on the substrate, as shown in

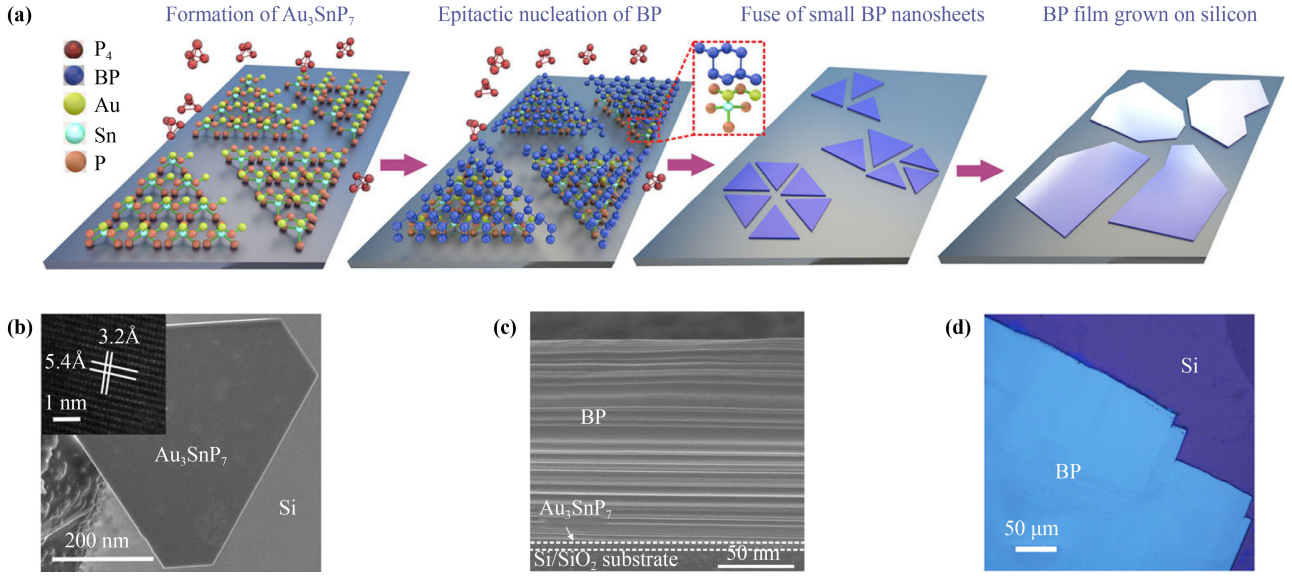

Fig. 9 **(a)** The figure shows the formation of Au_3SnP_7 on the substrate, the epitaxial growth of BP on Au_3SnP_7 into small nanosheets, and the fusion of small BP nanosheets on the substrate into large BP nanosheets. **(b)** SEM analysis of Au_3SnP_7 grown on the substrate, the inset shows the obtained HRTEM image of Au_3SnP_7. **(c)** The SEM of BP films grown on Au_3SnP_7. **(d)** Optical image of BP film grown on Si/SiO_2 substrate. Reproduced with permission from Ref. [89].

Fig. 9(a). The nucleation and growth of BP were further controlled by space-confined method. To achieve this, the intentional Au thin films were deposited on Si/SiO_2 substrates. After heating to 750°C, excess RP and Sn were wrapped in vacuum silica glass tubes to form distributed Au_3SnP_7 on Si/SiO_2 substrates. With the addition of SnI_4 as mineralizer, the nucleation and growth of BP films on Au_3SnP_7 mainly occurred at a lower holding temperature of 500 °C and further cooling stages. The scanning electron microscope studies were carried out to identify the Au_3SnP_7 nucleation seeds grown on Si/SiO_2 substrates, as shown in Fig. 9(b). As the cross-sectional TEM image shown in Fig. 9(c), BP has an obvious layered structure. With a proper control of the temperature gradient, the thickness as well as the lateral size of the BP film can be well under controlled [Fig. 9(d)]. The as-prepared BP thin films have good electrical properties, higher mobility and better on/off ratio compared with the exfoliated BP bulk crystals at room temperature.

Highly crystalline thin films of BP were synthesized on GaN substrates by adjusting the temperature parameters of growth, where RP was convert to BP at atmospheric pressure [90]. Furthermore, using the first-principles approach, they calculated the lattice mismatch energy between BP and GaN, and devised a method for epitaxial growth of BP thin films on GaN. It can be seen from the experimental and simulation results that GaN has adsorption effect of P atoms meanwhile P atoms have sufficient mobility on GaN. Thus, high-quality BP thin films can grow layer by layer on GaN. The length and width of the synthesized thin-film BP are in the range of 4–40 μm and 1–10 μm, respectively.

3.2 Pulsed laser deposition

Hao *et al.* [91] achieved the growth of centimeter-scale BP thin films in an ultra-high vacuum chamber by pulsed laser deposition (PLD) using bulk single-crystal BP as the source and mica with clean surfaces as the substrate, as shown in Fig. 10(a). PLD [92, 93] works by focusing high-intensity laser pulses on a raw material target in a vacuum environment. The surface area of the feedstock is vaporized, the laser spot strikes and ionizes the material, and the partially ionized free material is deposited on the substrate, which forms a thin film on the substrate. A controlled PLD strategy can be used to synthesize high-quality and few-layer BP at the centimeter scale [94]. Compared with bare mica, BP films prepared on mica have different reflection colors on mica, as shown in Fig. 10(b). Different from traditional thermal evaporation deposition, the application of pulsed laser can promote the formation of a large number of BP molecules in the transported physical vapor. Thus, the formation energy of the BP phase is reduced, which enables the large-scale growth of several layers of BP. Furthermore, by controlling the number of laser pulses in the deposition process, the film thickness can be controlled to a certain extent. The EDX spectrum of about ten-layer BP sample recorded by HAADF-TEM and the elemental mapping show the distribution of BP thin films. Therefore, the purity of the BP films is demonstrated, and the potential contamination by oxidation can be excluded. The EBSD mapping of the plane of the sample to determine its crystallinity, single crystal orientation and uniformity, as shown in Fig. 10(c). In addition, the preparation of field effect transistor (FET) arrays verifies the electrical properties of the as-grown BP, as shown in Fig. 10(d). According to the carrier mobility mapping results at different locations on the wafer, as shown in Fig. 10(e), the prepared BP films exhibited highly uniform electrical properties at the centimeter scale. The pulsed laser deposition for synthesizing black phosphorus has the following advantages. The BP film has the same composition as the target material source and is carried out in a vacuum environment. There is no phase transition involved and reduced impurity from other elements to pollution of the film which improved the quality of the film. High ionic kinetic energy can significantly enhance the 2D growth and inhibit the three-dimensional growth, which is more conducive to the preparation of thin films.

3.3 RP films transformation

The preparation of BP films can be realized under high temperature and high pressure conditions. Firstly, the RP film was deposited on the substrate, then the conversion of RP film to BP is realized under a certain temperature and pressure. As shown in Fig. 11(a), by using this experimental facility, a layer of RP film was deposited on the substrate. Place the substrate with the RP film in a quartz tube, then put Sn and SnI_4, under a certain temperature program, the conversion of RP film to BP film is realized [95], as shown in Fig. 11(b). In this way, BP with different thicknesses is directly grown on the silicon substrate, and the continuous area of BP film can reach 9000 μm^2. The SEM images of Figs. 11(c) and (d) can observe a large area of BP film.

Figure 11(e) summarizes the phase transition conditions for the synthesis of BP at different pressures and temperatures [96]. It can also realize the conversion which RP film to BP film at room temperature. Firstly, a layer of RP film was deposited on the substrate, and then converted into a BP film under pressure at room temperature, as shown in Fig. 11(f). The conversion process is carried out at room temperature, but achieving complete conversion from RP to BP at pressures over 8 GPa. The BP films also be prepared on sapphire at a certain temperature and pressure, as shown in Fig. 11(g). The deposition of RP on sapphire was achieved by using the apparatus shown in Fig. 11(h). Before deposition,

RP powder was charged into a quartz tube, then put it into a larger quartz tube and connected to a vacuum pump. The sapphire disk was placed in a quartz tube and was sealed with plastic wrap. In order to control the flow rate of the gas, the plastic wrap was punched a small hole, which the BP films can be synthesized at 700 °C and 1.5 GPa [97].

4 Conclusions and prospects

In this paper, the research progress in the preparation of BP is reviewed. BP is a very attractive 2D material, because of its unique crystal structure, it has excellent physical and chemical properties. It has shown great potential in many application fields, such as transistors, photodetectors, battery catalysis, biomedicine, sensors, etc. In order to meet the demand of high-throughput use in practical applications, the stable and facile preparation of BP is essential. The study on the growth mechanism of BP may promote the development of strategies for mass production of BP in high quality, especially the BP films. In the past few decades, some promising progresses have been made in improving the quality and

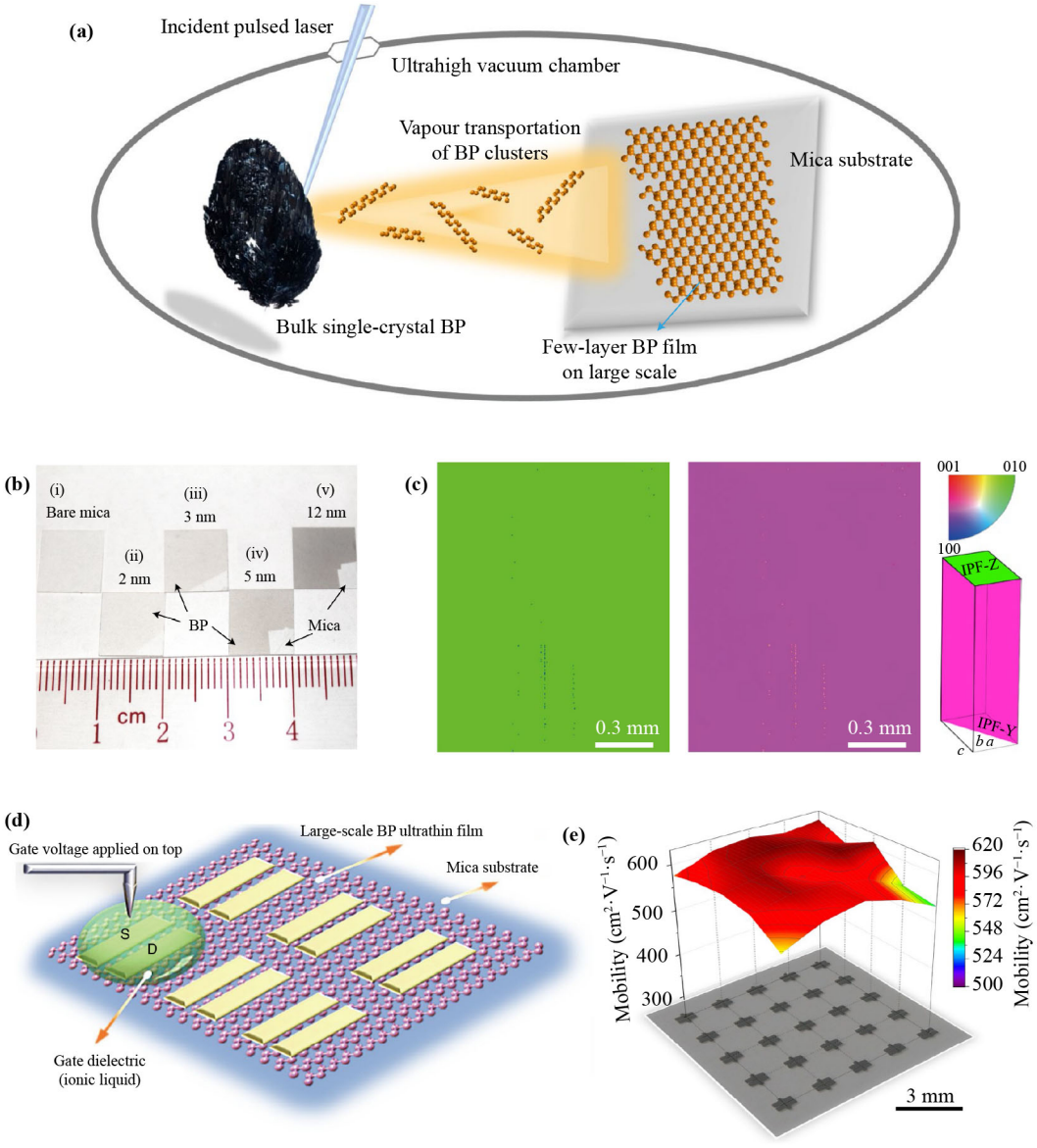

Fig. 10 **(a)** Schematic of the controlled PLD process used for the fabrication of few-layer BP films. **(b)** Photographs of bare mica (i) and deposited centimeter-scale BP films of different thicknesses (ii–v). **(c)** EBSD mapping shows that the prepared BP films have the same crystal orientation. **(d)** Schematic diagram of array top-gate field effect transistor with centimeter-scale few-layer BP grown on mica substrate. **(e)** Three-dimensional color map of carrier mobility at 250 K, extracted from 25 FETs fabricated with the same 5 nm BP sample, showing a highly uniform device performance. Reproduced with permission from Ref. [91].

yield of bulk BP crystals. This review mentions the high-temperature and high-pressure method from the beginning, the preparation of BP from flux, ball milling and the CVT methods, etc. A series of related studies on synthesis of BP are presented in Table 1. From the initial preparation of bulk BP to the controllable preparation of high-quality BP films, it is a big leap and challenge.

Although BP possess many novel properties, the instability in the air environment is a problem that needs to be solved. The rapid oxidation of BP in the environment affects its application. There are many methods have been proposed to protect BP, such as chemical modification, surface encapsulation and substitution doping. The chemical modification was an effective method to protect from erosion, the stability of BP was improved by the coordination between organic matter, such as aryl diazonium [98] and titanium sulfonate ligand [99]. The surface encapsulation refers to applying a passivation layer as an oxidation resistance. The passivation layer encapsulation is the most direct and effective method, some common protective layers are polymer, Al_2O_3 [100, 101], and SiO_2 [102]. The substitution doping can use various simple substances, such as tellurium (Te) or antimony (Sb) [103, 104], which can slow down the oxidization process.

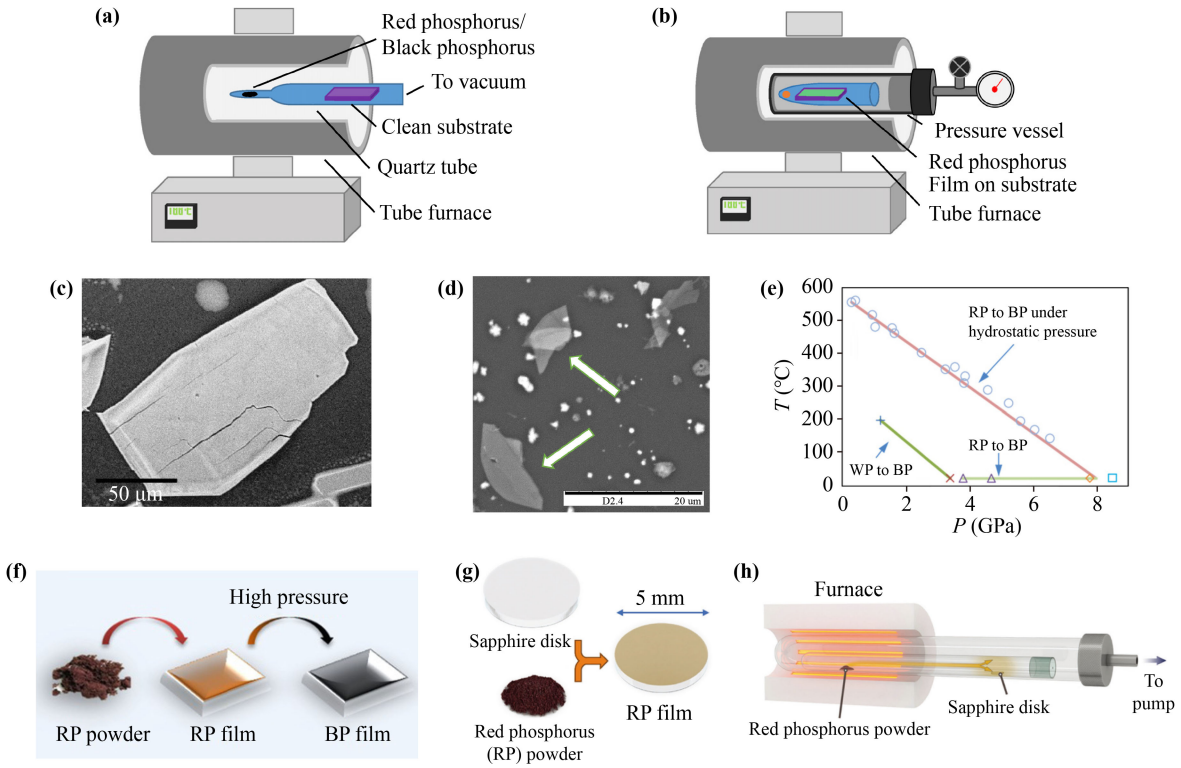

Fig. 11 **(a)** Schematic of amorphous RP thin film growth from vapor deposition. **(b)** Growth of BP film on the substrate from amorphous RP thin film. **(c, d)** SEM image of BP thin film sample on the substrate. **(e)** RP and BP conversion standards at different pressures and temperatures. **(f)** Strategy for the synthesis of thin BP films. **(g)** Schematic diagram of the preparation of RP films on sapphire. **(h)** Schematic diagram of the apparatus for depositing RP films on sapphire. Reproduced with permission from Ref. [95] (a–d), Ref. [96] (e, f) and Ref. [97] (g, h).

Table 1 Comparison of different methods of BP growth.

Method	Growth parameter	Morphology	Merits or faults	Ref.
HTHP	WP, 200 °C, 1.2 GPa, 30 mins WP, 200 °C, 1.3 GPa, few mins	bulk	complex experimental equipment and conditions	[92, 93]
Metal flux	WP and Hg, 370–410 °C, several days WP and Bi, 400 °C, 20 h	millimeter plate crystals	low purity and toxic	[61, 62]
Ball milling	WP, stainless steel ball, 1 h	powdery	low yield	[63]
Wet chemical	WP and ethylene diamine, 60–140 °C	sheet-like structure	mild reaction condition	[67]
Chemical vapor transport	RP/Sn/SnI_4, 650 °C RP/Au/SnI_4, 600 °C, 5–10 days Au film/Sn/SnI_4, 750 °C, 1 h	bulk or film	high quality crystals	[69, 70, 83]

We have tried to describe and analyze the corresponding mechanisms with different methods of preparing BP. PLD, HTHP and ball milling methods achieve a direct physical deposition of BP or phase transition from RP to BP, which require a large amount of energy. Metal flux, wet chemical and CVT methods, with additional chemical dynamic process, may reduce the external energy required for the growth of BP. Among these routes, a lot of effort has been made to explore the mechanisms of BP growth in the $Sn/I_2/P$ system. Both thermodynamic and kinetic factors were taken into account, such as the P:Sn:I ratio and growth temperature parameters (heating time, holding time, cooling time, etc.) [105]. The growth of BP occurs in the presence of molten Sn. While, other metals such as Pb can replace Sn in the reaction process. In the $Sn/I_2/P$ system, a ternary compound $Sn_{24}P_{19.3}I_8$ composed of Sn, I and P elements is believed to be the nucleation site of BP. Meanwhile, Sn and I elements play the role of transport agents. $Sn_{24}P_{19.3}I_8$ and HP co-existed, where HP is an allotrope of phosphorus. The existence of P vacancy in $Sn_{24}P_{19.3}I_8$ has become a critical reason for promoting the transformation of P_4 to HP. At present, the $Sn/I_2/P$ system is widely used to yield large amount of BP. However, the underlying nucleation and growth mechanism is still unclear. Additional efforts are still needed to reveal the conversion from RP to BP in the process.

Referring to the experience of traditional crystal epitaxy, the large-area growth of two-dimensional materials will also be affected by the lattice matching between two-dimensional materials and substrates. After solving the problems of nucleation and lattice orientation, it is expected to form large-area epitaxy. For example, some growth methods have been explored by using factors such as step edge. The ladder growth mechanism may enable the large-scale production of high-quality thin film BP, for example to achieve epitaxial growth of thin film BP on 2D materials such as GaN.

We hope that through some understanding of the growth mechanisms in this review, it could be helpful for BP growth especially the BP films growth in high quality and in a controllable way.

Acknowledgements This work was supported by the National Key R&D Program of China (No. 2021YFA1200804), the National Natural Science Foundation of China (Grant Nos. 61922082, 61875223, and 61927813). The support from the Vacuum Interconnected Nanotech Workstation (Nano-X) of Suzhou Institute of Nano-tech and Nano-bionics (SINANO), Chinese Academy of Sciences is also acknowledged.

References

1. A. Pfitzner, M. F. Brau, J. Zweck, G. Brunklaus, and H. Eckert, Phosphorus nanorods-two allotropic modifications of a long-known element, *Angew. Chem. Int. Ed.* 43(32), 4228 (2004)
2. F. Bachhuber, J. von Appen, R. Dronskowski, P. Schmidt, T. Nilges, A. Pfitzner, and R. Weihrich, Die erweiterte stabilitätsreihe der phosphorallotropee, *Angew. Chem.* 126(43), 11813 (2014)
3. M. Ruck, D. Hoppe, B. Wahl, P. Simon, Y. Wang, and G. Seifert, Faserförmiger roter phosphor, *Angew. Chem.* 117(46), 7788 (2005)
4. N. Eckstein, A. Hohmann, R. Weihrich, T. Nilges, and P. Schmidt, Synthesis and phase relations of single-phase fibrous phosphorus, *Z. Anorg. Allg. Chem.* 639(15), 2741 (2013)
5. G. Natta and L. Passerini, The crystal structure of white phosphorus, *Nature* 125(3158), 707 (1930)
6. R. L. Keiter and C. P. Gamage, Combustion of white phosphorus, *J. Chem. Educ.* 78(7), 908 (2001)
7. S. Zhang, H. J. Qian, Z. Liu, H. Ju, Z. Y. Lu, H. Zhang, L. Chi, and S. Cui, Towards unveiling the exact molecular structure of amorphous red phosphorus by single-molecule studies, *Angew. Chem. Int. Ed.* 58(6), 1659 (2019)
8. C. M. Fung, C. C. Er, L. L. Tan, A. R. Mohamed, and S. P. Chai, Red Phosphorus: An Up-and-Coming Photocatalyst on the Horizon for Sustainable Energy Development and Environmental Remediation, *Chem. Rev.* 122(3), 3879 (2022)
9. Z. Sun, B. Zhang, Y. Zhao, M. Khurram, and Q. Yan, Synthesis, exfoliation, and transport properties of quasi-1D van der Waals fibrous red phosphorus, *Chem. Mater.* 33(15), 6240 (2021)
10. Z. Zhu, P. Cui, X. Cai, M. Xia, Y. Jia, S. Zhang, and Z. Zhang, Red phosphorus in its two-dimensional limit: Novel clathrates with varying band gaps and superior chemical stabilities, *Nanoscale* 10(29), 13969 (2018)
11. W. Hittorf, Zur Kenntniss des Phosphors, *Annalen der Physik und Chemie* 202(10), 193 (1865)
12. L. Zhang, H. Huang, Z. Lv, L. Li, M. Gu, X. Zhao, B. Zhang, Y. Cheng, and J. Zhang, Phonon properties of bulk violet phosphorus single crystals: Temperature and pressure evolution, *ACS Appl. Electron. Mater.* 3(3), 1043 (2021)
13. L. Zhang, H. Huang, B. Zhang, M. Gu, D. Zhao, X. Zhao, L. Li, J. Zhou, K. Wu, Y. Cheng, and J. Zhang, Structure and properties of violet phosphorus and its phosphorene exfoliation, *Angew. Chem. Int. Ed.* 59(3), 1074 (2020)
14. L. Zhang, M. Gu, L. Li, X. Zhao, C. Fu, T. Liu, X. Xu, Y. Cheng, and J. Zhang, High yield synthesis of violet phosphorus crystals, *Chem. Mater.* 32(17), 7363 (2020)
15. R. Zhao, S. Liu, X. Zhao, M. Gu, Y. Zhang, M. Jin, Y. Wang, Y. Cheng, and J. Zhang, Violet phosphorus quantum dots, *J. Mater. Chem. A* 10(1), 245 (2021)
16. X. Chen, J. S. Ponraj, D. Fan, and H. Zhang, An overview of the optical properties and applications of black phosphorus, *Nanoscale* 12(6), 3513 (2020)
17. R. Gusmão, Z. Sofer, and M. Pumera, Black phosphorus rediscovered: From bulk material to monolayers, *Angew. Chem. Int. Ed.* 56(28), 8052 (2017)
18. J. C. Jamieson, Crystal structures adopted by black phosphorus at high pressures, *Science* 139(356), 1291

(1963)
19. W. Lei, G. Liu, J. Zhang, and M. Liu, Black phosphorus nanostructures: Recent advances in hybridization, doping and functionalization, *Chem. Soc. Rev.* 46(12), 3492 (2017)
20. P. W. Bridgman, Two new modifications of phosphorus, *J. Am. Chem. Soc.* 36(7), 1344 (1914)
21. B. M. L. P. A. G. O'hare, B. M. Lewis, and I. Shirotani, Thermodynamic stability of orthorhombic black phosphorus, *Thermochim. Acta* 129(1), 57 (1988)
22. M. Zhao, H. Qian, X. Niu, W. Wang, L. Guan, J. Sha, and Y. Wang, Growth mechanism and enhanced yield of black phosphorus microribbons, *Cryst. Growth Des.* 16(2), 1096 (2016)
23. L. Li, Y. Yu, G. J. Ye, Q. Ge, X. Ou, H. Wu, D. Feng, X. H. Chen, and Y. Zhang, Black phosphorus field-effect transistors, *Nat. Nanotechnol.* 9(5), 372 (2014)
24. V. Tran, R. Soklaski, Y. Liang, and L. Yang, Layer-controlled band gap and anisotropic excitons in few-layer black phosphorus, *Phys. Rev. B* 89(23), 235319 (2014)
25. X. Liu, K. W. Ang, W. Yu, J. He, X. Feng, Q. Liu, H. Jiang, Dan Tang, J. Wen, Y. Lu, W. Liu, P. Cao, S. Han, J. Wu, W. Liu, X. Wang, D. Zhu, and Z. He, Black phosphorus based field effect transistors with simultaneously achieved near ideal subthreshold swing and high hole mobility at room temperature, *Sci. Rep.* 6(1), 24920 (2016)
26. G. Long, D. Maryenko, J. Shen, S. Xu, J. Hou, Z. Wu, W. K. Wong, T. Han, J. Lin, Y. Cai, R. Lortz, and N. Wang, Achieving ultrahigh carrier mobility in two-dimensional hole gas of black phosphorus, *Nano Lett.* 16(12), 7768 (2016)
27. Y. Xu, J. Yuan, K. Zhang, Y. Hou, Q. Sun, Y. Yao, S. Li, Q. Bao, H. Zhang, and Y. Zhang, Field-induced N-doping of black phosphorus for CMOS compatible 2D logic electronics with high electron mobility, *Adv. Funct. Mater.* 27(38), 1702211 (2017)
28. X. Feng, X. Huang, L. Chen, W. C. Tan, L. Wang, and K. W. Ang, High mobility anisotropic black phosphorus nanoribbon field-effect transistor, *Adv. Funct. Mater.* 28(28), 1801524 (2018)
29. G. Wang, Z. Guo, C. Chen, W. Yu, B. Xu, and B. Lin, Exploring a high-carrier-mobility black phosphorus/$MoSe_2$ heterostructure for high-efficiency thin film solar cells, *Sol. Energy* 236, 576 (2022)
30. M. Buscema, D. J. Groenendijk, S. I. Blanter, G. A. Steele, H. S. van der Zant, and A. Castellanos-Gomez, Fast and broadband photoresponse of few-layer black phosphorus field-effect transistors, *Nano Lett.* 14(6), 3347 (2014)
31. W. Zhu, M. N. Yogeesh, S. Yang, S. H. Aldave, J. S. Kim, S. Sonde, L. Tao, N. Lu, and D. Akinwande, Flexible black phosphorus ambipolar transistors, circuits and AM demodulator, *Nano Lett.* 15(3), 1883 (2015)
32. Z. Sobiesierski and R. T. Phillips, A time-resolved photoluminescence study of amorphous phosphorus, *Solid State Commun.* 60(1), 25 (1986)
33. R. J. Suess, J. D. Hart, E. Leong, M. Mittendorff, and T. E. Murphy, Black phosphorus frequency mixer for infrared optoelectronic signal processing, *APL Photonics* 4(3), 034502 (2019)
34. G. Hu, T. Albrow-Owen, X. Jin, A. Ali, Y. Hu, R. C. T. Howe, K. Shehzad, Z. Yang, X. Zhu, R. I. Woodward, T. C. Wu, H. Jussila, J. B. Wu, P. Peng, P. H. Tan, Z. Sun, E. J. R. Kelleher, M. Zhang, Y. Xu, and T. Hasan, Black phosphorus ink formulation for inkjet printing of optoelectronics and photonics, *Nat. Commun.* 8(1), 278 (2017)
35. X. Chen, X. Lu, B. Deng, O. Sinai, Y. Shao, C. Li, S. Yuan, V. Tran, K. Watanabe, T. Taniguchi, D. Naveh, L. Yang, and F. Xia, Widely tunable black phosphorus mid-infrared photodetector, *Nat. Commun.* 8(1), 1672 (2017)
36. M. Valt, M. Caporali, B. Fabbri, A. Gaiardo, S. Krik, E. Iacob, L. Vanzetti, C. Malagu, M. Banchelli, C. D' Andrea, M. Serrano-Ruiz, M. Vanni, M. Peruzzini, and V. Guidi, Air stable nickel-decorated black phosphorus and its room-temperature chemiresistive gas sensor capabilities, *ACS Appl. Mater. Interfaces* 13(37), 44711 (2021)
37. D. An, X. Zhang, Z. Bi, W. Shan, H. Zhang, S. Xia, and M. Qiu, Low-dimensional black phosphorus in sensor applications: Advances and challenges, *Adv. Funct. Mater.* 31(52), 2106484 (2021)
38. J. Sun, Y. Sun, M. Pasta, G. Zhou, Y. Li, W. Liu, F. Xiong, and Y. Cui, Entrapment of polysulfides by a black-phosphorus-modified separator for lithium-sulfur batteries, *Adv. Mater.* 28(44), 9797 (2016)
39. Y. Wang, M. He, S. Ma, C. Yang, M. Yu, G. Yin, and P. Zuo, Low-temperature solution synthesis of black phosphorus from red phosphorus: Crystallization mechanism and lithium ion battery applications, *J. Phys. Chem. Lett.* 11(7), 2708 (2020)
40. J. Zhu, G. Xiao, and X. Zuo, Two-dimensional black phosphorus: An emerging anode material for lithium-ion batteries, *Nano-Micro Lett.* 12(1), 120 (2020)
41. L. Bai, X. Wang, S. Tang, Y. Kang, J. Wang, Y. Yu, Z. K. Zhou, C. Ma, X. Zhang, J. Jiang, P. K. Chu, and X. F. Yu, Black phosphorus/platinum heterostructure: A highly efficient photocatalyst for solar-driven chemical reactions, *Adv. Mater.* 30(40), 1803641 (2018)
42. J. Miao, L. Zhang, and C. Wang, Black phosphorus electronic and optoelectronic devices, *2D Mater.* 6(3), 032003 (2019)
43. T. Yin, L. Long, X. Tang, M. Qiu, W. Liang, R. Cao, Q. Zhang, D. Wang, and H. Zhang, Advancing applications of black phosphorus and BP-analog materials in photo/electrocatalysis through structure engineering and surface modulation, *Adv. Sci. (Weinh.)* 7(19), 2001431 (2020)
44. L. Zhang, B. Wang, Y. Zhou, C. Wang, X. Chen, and H. Zhang, Synthesis techniques, optoelectronic properties, and broadband photodetection of thin-film black phosphorus, *Adv. Opt. Mater.* 8(15), 2000045 (2020)
45. Z. Xie, M. Peng, R. Lu, X. Meng, W. Liang, Z. Li, M. Qiu, B. Zhang, G. Nie, N. Xie, H. Zhang, and P. N.

Prasad, Black phosphorus-based photothermal therapy with aCD47-mediated immune checkpoint blockade for enhanced cancer immunotherapy, *Light Sci. Appl.* 9(1), 161 (2020)

46. C. Xing, S. Chen, M. Qiu, X. Liang, Q. Liu, Q. Zou, Z. Li, Z. Xie, D. Wang, B. Dong, L. Liu, D. Fan, and H. Zhang, Conceptually novel black phosphorus/cellulose hydrogels as promising photothermal agents for effective cancer therapy, *Adv. Healthc. Mater.* 7(7), 1701510 (2018)
47. F. Yin, K. Hu, S. Chen, D. Wang, J. Zhang, M. Xie, D. Yang, M. Qiu, H. Zhang, and Z. G. Li, Black phosphorus quantum dot based novel siRNA delivery systems in human pluripotent teratoma PA-1 cells, *J. Mater. Chem. B* 5(27), 5433 (2017)
48. J. O. Island, G. A. Steele, H. S. J. v. d. Zant, and A. Castellanos-Gomez, Environmental instability of few-layer black phosphorus, *2D Mater.* 2(1), 011002 (2015)
49. Y. Y. Illarionov, M. Waltl, G. Rzepa, J. S. Kim, S. Kim, A. Dodabalapur, D. Akinwande, and T. Grasser, Long-term stability and reliability of black phosphorus field-effect transistors, *ACS Nano* 10(10), 9543 (2016)
50. D. K. Sang, H. Wang, Z. Guo, N. Xie, and H. Zhang, Recent developments in stability and passivation techniques of phosphorene toward next-generation device applications, *Adv. Funct. Mater.* 29(45), 1903419 (2019)
51. A. Favron, E. Gaufres, F. Fossard, A. L. Phaneuf-L'Heureux, N. Y. Tang, P. L. Levesque, A. Loiseau, R. Leonelli, S. Francoeur, and R. Martel, Photooxidation and quantum confinement effects in exfoliated black phosphorus, *Nat. Mater.* 14(8), 826 (2015)
52. G. Kim, D. Kim, Y. Choi, A. Ghorai, G. Park, and U. Jeong, New approaches to produce large-area single crystal thin films, *Adv. Mater.* 35(4), 2203373 (2022)
53. A. Zavabeti, A. Jannat, L. Zhong, A. A. Haidry, Z. Yao, and J. Z. Ou, Two-dimensional materials in large-areas: Synthesis, properties and applications, *Nano-Micro Lett.* 12(1), 66 (2020)
54. K. S. Novoselov, D. Jiang, F. Schedin, T. J. Booth, V. V. Khotkevich, S. V. Morozov, and A. K. Geim, Two-dimensional atomic crystals, *Proc. Natl. Acad. Sci. USA* 102(30), 10451 (2005)
55. H. Liu, A. T. Neal, Z. Zhu, Z. Luo, X. Xu, D. Tománek, and P. D. Ye, Phosphorene: An unexplored 2D semiconductor with a high hole mobility, *ACS Nano* 8(4), 4033 (2014)
56. W. Lu, H. Nan, J. Hong, Y. Chen, C. Zhu, Z. Liang, X. Ma, Z. Ni, C. Jin, and Z. Zhang, Plasma-assisted fabrication of monolayer phosphorene and its Raman characterization, *Nano Res.* 7(6), 853 (2014)
57. J. Kang, S. A. Wells, J. D. Wood, J.-H. Lee, X. Liu, C. R. Ryder, J. Zhu, Jeffrey R Guest, C. A. Husko, and M. C. Hersam, Stable aqueous dispersions of optically and electronically active phosphorene, *Proc. Natl. Acad. Sci. USA* 113(42), 11688 (2016)
58. D. Hanlon, C. Backes, E. Doherty, C. S. Cucinotta, N. C. Berner, C. Boland, K. Lee, A. Harvey, P. Lynch, Z. Gholamvand, S. Zhang, K. Wang, G. Moynihan, A. Pokle, Q. M. Ramasse, N. McEvoy, W. J. Blau, J. Wang, G. Abellan, F. Hauke, A. Hirsch, S. Sanvito, D. D. O'Regan, G. S. Duesberg, V. Nicolosi, and J. N. Coleman, Liquid exfoliation of solvent-stabilized few-layer black phosphorus for applications beyond electronics, *Nat. Commun.* 6(1), 8563 (2015)
59. P. Yasaei, B. Kumar, T. Foroozan, C. Wang, M. Asadi, D. Tuschel, J. E. Indacochea, R. F. Klie, and A. Salehi-Khojin, High-quality black phosphorus atomic layers by liquid-phase exfoliation, *Adv. Mater.* 27(11), 1887 (2015)
60. X. Wang, A. M. Jones, K. L. Seyler, V. Tran, Y. Jia, H. Zhao, H. Wang, L. Yang, X. Xu, and F. Xia, Highly anisotropic and robust excitons in monolayer black phosphorus, *Nat. Nanotechnol.* 10, 517 (2015)
61. L. Q. Sun, M. J. Li, K. Sun, S. H. Yu, R. S. Wang, and H. M. Xie, Electrochemical activity of black phosphorus as an anode material for lithium-ion batteries, *J. Phys. Chem. C* 116(28), 14772 (2012)
62. N. Antonatos, D. Bousa, S. Shcheka, S. M. Beladi-Mousavi, M. Pumera, and Z. Sofer, *In situ* doping of black phosphorus by high-pressure synthesis, *Inorg. Chem.* 58(15), 10227 (2019)
63. H. Xiang, Y. T. Nie, H. C. Zheng, X. H. Sun, X. L. Sun, and Y. Song, The mechanism of structural changes and crystallization kinetics of amorphous red phosphorus to black phosphorus under high pressure, *Chem. Commun. (Camb.)* 55(56), 8094 (2019)
64. Y. Akahama, M. Miyakawa, T. Taniguchi, A. Sano-Furukawa, S. Machida, and T. Hattori, Structure refinement of black phosphorus under high pressure, *J. Chem. Phys.* 153(1), 014704 (2020)
65. J. K. Burdett, and S. Lee, The pressure-induced black phosphorus to A7 (arsenic) phase transformation: An analysis using the concept of orbital symmetry conservation, *J. Solid State Chem.* 44(3), 415 (1982)
66. D. Scelta, A. Baldassarre, M. Serrano-Ruiz, K. Dziubek, A. B. Cairns, M. Peruzzini, R. Bini, and M. Ceppatelli, Interlayer bond formation in black phosphorus at high pressure, *Angew. Chem. Int. Ed.* 56, 14135 (2017)
67. H. Krebs, H. Weitz, and K. H. Worms, Über die struktur und die eigenschaften der halbmetalle. VIII. Die katalytische darstellung des schwarzen phosphors, *Z. Anorg. Allg. Chem.* 280(1–3), 119 (1955)
68. M. Baba, F. Izumida, Y. Takeda, and A. Morita, Preparation of black phosphorus single crystals by a completely closed bismuth-flux method and their crystal morphology, *Jpn. J. Appl. Phys.* 28(6R), 1019 (1989)
69. M. Nagao, A. Hayashi, and M. Tatsumisago, All-solid-state lithium secondary batteries with high capacity using black phosphorus negative electrode, *J. Power Sources* 196(16), 6902 (2011)
70. F. Zhou, L. Ouyang, M. Zeng, J. Liu, H. Wang, H. Shao, and M. Zhu, Growth mechanism of black phosphorus synthesized by different ball milling techniques, *J. Alloys Compd.* 784, 339 (2019)
71. X. Zhu, T. Zhang, Z. Sun, H. Chen, J. Guan, X. Chen, H. Ji, P. Du, and S. Yang, Black phosphorus revisited:

A missing metal-free elemental photocatalyst for visible light hydrogen evolution, *Adv. Mater.* 29(17), 1605776 (2017)

72. N. V. Chien, H. Shin, and J. Y. Song, Sn-assisted solid state crystallization of red phosphorus to black phosphorus, *Scr. Mater.* 177, 128 (2020)
73. B. Tian, B. Tian, B. Smith, M. C. Scott, Q. Lei, R. Hua, Y. Tian, and Y. Liu, Facile bottom-up synthesis of partially oxidized black phosphorus nanosheets as metal-free photocatalyst for hydrogen evolution, *Proc. Natl. Acad. Sci. USA* 115(17), 4345 (2018)
74. B. Tian, B. Tian, B. Smith, M. C. Scott, R. Hua, Q. Lei, and Y. Tian, Supported black phosphorus nanosheets as hydrogen-evolving photocatalyst achieving 5.4% energy conversion efficiency at 353 K, *Nat. Commun.* 9(1), 1397 (2018)
75. T. Nilges, M. Kersting, and T. Pfeifer, A fast low-pressure transport route to large black phosphorus single crystals, *J. Solid State Chem.* 181(8), 1707 (2008)
76. S. Lange, P. Schmidt, and T. Nilges, Au_3SnP_7@black phosphorus: An easy access to black phosphorus, *Inorg. Chem.* 46(10), 4028 (2007)
77. F. T. Johra and W. G. Jung, Synthesis of black phosphorus via a facile vapor transfer method, *Electron. Mater. Lett.* 15(5), 639 (2019)
78. N. Izquierdo, J. C. Myers, N. C. A. Seaton, S. K. Pandey, and S. A. Campbell, Thin-film deposition of surface passivated black phosphorus, *ACS Nano* 13(6), 7091 (2019)
79. M. Wentink, J. Gaberle, M. Aghajanian, A. A. Mostofi, N. J. Curson, J. Lischner, S. R. Schofield, A. L. Shluger, and A. J. Kenyon, Substitutional tin acceptor states in black phosphorus, *J. Phys. Chem. C* 125(41), 22883 (2021)
80. N. Antonatos, J. Sturala, V. Mazanek, D. Sedmidubsky, M. Vesely, K. Ruzicka, J. Hejtmanek, P. Levinsky, and Z. Sofer, Black phosphorus: Fundamental properties and influence of impurities induced by its synthesis, *ACS Appl. Mater. Interfaces* 14(30), 34867 (2022)
81. Q. Xu, Y. Zhu, C. Shi, N. Zhang, and T. Xie, The preparation of black phosphorus in RP/Sn/I_2 system: its nucleation agent and relatively optimal temperature program, *J. Mater. Sci. Mater. Electron.* 31(21), 19093 (2020)
82. M. M. Shatruk, K. A. Kovnir, A. V. Shevelkov, I. A. Presniakov, and B. A. Popovkin, First tin pnictide halides $Sn_{24}P_{19.3}I_8$ and $Sn_{24}As_{19.3}I_8$: Synthesis and the clathrate-i type of the crystal structure, *Inorg. Chem.* 38(15), 3455 (1999)
83. V. V. Novikov, A. V. Matovnikov, D. V. Avdashchenko, N. V. Mitroshenkov, E. Dikarev, S. Takamizawa, M. A. Kirsanova, and A. V. Shevelkov, Low-temperature structure and lattice dynamics of the thermoelectric clathrate $Sn_{24}P_{19.3}I_8$, *J. Alloys Compd.* 520, 174 (2012)
84. S. Li, X. Liu, X. Fan, Y. Ni, J. Miracle, N. Theodoropoulou, J. Sun, S. Chen, B. Lv, and Q. Yu, New strategy for black phosphorus crystal growth through ternary clathrate, *Cryst. Growth Des.* 17(12), 6579 (2017)
85. Z. Chen, Y. Zhu, J. Lei, W. Liu, Y. Xu, and P. Feng, A stage-by-stage phase-induction and nucleation of black phosphorus from red phosphorus under low-pressure mineralization, *CrystEngComm* 19(47), 7207 (2017)
86. Z. Zhang, D. H. Xing, J. Li, and Q. Yan, Hittorf's phosphorus: The missing link during transformation of red phosphorus to black phosphorus, *CrystEngComm* 19(6), 905 (2017)
87. G. Tiouitchi, M. A. Ali, A. Benyoussef, M. Hamedoun, A. Lachgar, M. Benaissa, A. Kara, A. Ennaoui, A. Mahmoud, F. Boschini, H. Oughaddou, A. El Kenz, and O. Mounkachi, An easy route to synthesize high-quality black phosphorus from amorphous red phosphorus, *Mater. Lett.* 236, 56 (2019)
88. Y. Yu, B. Xing, D. Wang, L. Guan, X. Niu, J. Yao, X. Yan, S. Zhang, Y. Liu, X. Wu, J. Sha, and Y. Wang, Improvement in the quality of black phosphorus by selecting a mineralizer, *Nanoscale* 11(42), 20081 (2019)
89. Y. Xu, X. Shi, Y. Zhang, H. Zhang, Q. Zhang, Z. Huang, X. Xu, J. Guo, H. Zhang, L. Sun, Z. Zeng, A. Pan, and K. Zhang, Epitaxial nucleation and lateral growth of high-crystalline black phosphorus films on silicon, *Nat. Commun.* 11(1), 1330 (2020)
90. D. Han, Q. Liu, Q. Zhang, J. Ji, S. Sang, and B. Xu, Synthesis of highly crystalline black phosphorus thin films on GaN, *Nanoscale* 12(48), 24429 (2020)
91. Z. Wu, Y. Lyu, Y. Zhang, R. Ding, B. Zheng, Z. Yang, S. P. Lau, X. H. Chen, and J. Hao, Large-scale growth of few-layer two-dimensional black phosphorus, *Nat. Mater.* 20(9), 1203 (2021)
92. P. R. Willmott and J. R. Huber, Pulsed laser vaporization and deposition, *Rev. Mod. Phys.* 72(1), 315 (2000)
93. Z. Yang and J. Hao, Progress in pulsed laser deposited two-dimensional layered materials for device applications, *J. Mater. Chem. C* 4(38), 8859 (2016)
94. Z. Yang, J. Hao, S. Yuan, S. Lin, H. M. Yau, J. Dai, and S. P. Lau, Field-effect transistors based on amorphous black phosphorus ultrathin films by pulsed laser deposition, *Adv. Mater.* 27(25), 3748 (2015)
95. J. B. Smith, D. Hagaman, and H. F. Ji, Growth of 2D black phosphorus film from chemical vapor deposition, *Nanotechnology* 27(21), 215602 (2016)
96. X. Li, B. Deng, X. Wang, S. Chen, M. Vaisman, S.-I. Karato, G. Pan, M. L. Lee, J. Cha, H. Wang, and F. Xia, Synthesis of thin-film black phosphorus on a flexible substrate, *2D Mater.* 2(3), 031002 (2015)
97. C. Li, Y. Wu, B. Deng, Y. Xie, Q. Guo, S. Yuan, X. Chen, M. Bhuiyan, Z. Wu, K. Watanabe, T. Taniguchi, H. Wang, J. J. Cha, M. Snure, Y. Fei, and F. Xia, Synthesis of crystalline black phosphorus thin film on sapphire, *Adv. Mater.* 30(6), 1703748 (2018)
98. C. R. Ryder, J. D. Wood, S. A. Wells, Y. Yang, D. Jariwala, T. J. Marks, G. C. Schatz, and M. C. Hersam, Covalent functionalization and passivation of exfoliated black phosphorus via aryl diazonium chemistry, *Nat. Chem.* 8(6), 597 (2016)
99. Y. Zhao, H. Wang, H. Huang, Q. Xiao, Y. Xu, Z. Guo,

H. Xie, J. Shao, Z. Sun, W. Han, X. F. Yu, P. Li, and P. K. Chu, Surface coordination of black phosphorus for robust air and water stability, *Angew. Chem. Int. Ed.* 16(55), 5003 (2016)

100. Y. Y. Illarionov, M. Waltl, G. Rzepa, T. Knobloch, J. S. Kim, D. Akinwande, and T. Grasser, Highly-stable black phosphorus field-effect transistors with low density of oxide traps, *npj 2D Mater. Appl.* 1(1) (2017)
101. J. D. Wood, S. A. Wells, D. Jariwala, K. S. Chen, E. Cho, V. K. Sangwan, X. Liu, L. J. Lauhon, T. J. Marks, and M. C. Hersam, Effective passivation of exfoliated black phosphorus transistors against ambient degradation, *Nano Lett.* 14(12), 6964 (2014)
102. B. Wan, B. Yang, Y. Wang, J. Zhang, Z. Zeng, Z. Liu, and W. Wang, Enhanced stability of black phosphorus field-effect transistors with SiO_2 passivation, *Nanotechnology* 26(43), 435702 (2015)
103. Y. Xu, J. Yuan, L. Fei, X. Wang, Q. Bao, Y. Wang, K. Zhang, and Y. Zhang, Selenium-doped black phosphorus for high-responsivity 2D photodetectors, *Small* 12(36), 5000 (2016)
104. B. Yang, B. Wan, Q. Zhou, Y. Wang, W. Hu, W. Lv, Q. Chen, Z. Zeng, F. Wen, J. Xiang, S. Yuan, J. Wang, B. Zhang, W. Wang, J. Zhang, B. Xu, Z. Zhao, Y. Tian, and Z. Liu, Te-doped black phosphorus field-effect transistors, *Adv. Mater.* 28(42), 9408 (2016)
105. M. Zhao, X. Niu, L. Guan, H. Qian, W. Wang, J. Sha, and Y. Wang, Understanding the growth of black phosphorus crystals, *CrystEngComm* 18(40), 7737 (2016)